Available online at www.sciencedirect.com
ScienceDirect
Journal of Sound and Vibration 320 (2009) 472–481
JOURNAL OF SOUND AND VIBRATION
www.elsevier.com/locate/jsvi

Rapid Communication

Real-time anti-node visualization of vibrating distributed systems in noisy environments using defocused laser speckle contrast analysis

Lionel Keene[a,*], Fu-Pen Chiang[b]

[a]*Getty Conservation Institute, 1200 Getty Center Drive, Suite 700, Los Angeles, CA 90049-1684, USA*
[b]*Department of Mechanical Engineering, State University of New York at Stony Brook, Stony Brook, NY 11794-2300, USA*

Received 8 January 2008; received in revised form 25 June 2008; accepted 20 August 2008
Handling Editor: S. Bolton
Available online 28 November 2008

Abstract

A simple optical technique is described that allows for the direct whole-field visualization of anti-nodal patterns in noisy environments. The technique involves the combination of defocused laser speckle imaging with the laser speckle contrast analysis (LASCA) algorithm to relate local contrast reduction of a laser speckle pattern to the magnitude of the gradient vectors that arise due to the tilt deflection of a vibrating surface. The method requires no reference beam and is tolerant of environmental noise. The sensitivity of the technique is a direct function of the degree of defocus of the speckle pattern and thus can be readily adjusted. By ratioing the instantaneous contrast to the reference image contrast, a simple method for thresholding the noise floor (noise at reference state) is attained, thus increasing the method's tolerance to ambient disturbances. Results from forced vibration via acoustic excitation of a square and rectangular membrane—with and without simultaneous white noise excitation—are shown. Results are compared to theoretical predictions for an ideal membrane, with good agreement.

1. Introduction

Optical interferometry—as a form of metrology—is a mature family of techniques frequently applied to engineering problems that require a sensitive, full field and non-contact method of measurement [1]. They are particularly useful for spatially characterizing the virbratory response of distributed systems such as membranes and plates [1,2]. These techniques generally fall into two branches of interferometry, namely holography and speckle interferometry. Of these, holography is the technique of choice when very high sensitivity and spatial resolution are required. The high sensitivity of the holographic method (of the order of half a wavelength of the illuminating light) is simultaneously one of its major drawbacks, as it has a very low tolerance for environmental disturbances and requires a very stable and controlled experimental setup during

*Corresponding author.
E-mail address: lkeene@getty.edu (L. Keene).

0022-460X/$ - see front matter © 2008 Published by Elsevier Ltd.
doi:10.1016/j.jsv.2008.08.022

application. As such, holography can be very difficult to apply "in the field" or in situations where an appreciable degree of ambient noise (large thermal fluctuations, background vibration, etc.) exists.

The sister technique to holography is laser speckle interferometry. These techniques make use of the speckle pattern generated by the microrelief of a surface when illuminated by a coherent light source. They exploit the phase information contained in the optical wavefront to obtain displacement information parallel and/or orthogonal to the optical axis, in which case they are considered to be true interferometers [1,3]. While sensitivity can approach that of holography, they also suffer a decrease in robustness when used in experimentally noisy conditions. In addition, many of these methods require the application of a phase-unwrapping post-processing step, the unwrapping procedure itself being a notoriously ill-defined problem and often difficult to perform on noisy phase maps [4]. Attempts have been made to compensate for sources of optical noise (i.e. thermal, speckle, etc., see for example Ref. [5]), but these techniques are of limited value when the baseline mechanical noise is of an amplitude of the order of the sensitivity of the particular method. To answer some of these criticisms of complexity and sensitivity to noise and disturbance, alternatives to the previously mentioned methods for visualizing the nodes/anti-nodes by laser speckle have been presented in the literature. These methods—not necessarily interferometers in the truest sense—exploit the optical decorrelation between reference and object speckle patterns either through a direct measure of the cross-correlation of speckle patterns, through the formation of correlation fringes, or by visible contrast reduction through time-average imaging of some surface under dynamic motion. In the case of a quantitative decorrelation analysis, two or more images are numerically cross-correlated via digital computer and the localized decorrelation is used as a relative metric to gauge the magnitude of some physical process [6–10]. Alternatively, a time-average optical cross-correlation can be performed by overlapping the speckle pattern from the object beam with the speckle pattern from a reference beam and visually monitoring the brightness field to locate fringes. Chiang and Juang [11–14] were the first to exploit the sensitivity of a *defocused* speckle pattern to vibrating surfaces as a measuring tool and demonstrated its application to vibrating plates and beams. More recent studies include those of Spagnolo et al. [15,16]. However, numerical cross-correlation is computationally expensive, while optical correlation requires the additional complexity of a reference beam. Both techniques are sensitive to mechanical noise that can obscure the signal of interest. Hung [17–19] pioneered the application of digital shearography, a method that employs a shearing camera to generate two pairs of optically sheared speckle patterns, which are made to interfere via digital computer image processing. The technique is notable for its greatly enhanced tolerance of noise relative to more traditional interferometric techniques. Along these lines, Gregory [20] investigated the use of a simple defocused speckle photography method for visualizing surface tilts. Following the method of Tiziani [21] (who showed that when a surface was illuminated by a *collimated* coherent light source there exists a focal plane behind the imaging lens wherein the in-plane displacements and out-of-plane tilt motions of the speckles become decoupled), Gregory extended the method to diverging illumination and showed in that case that the decoupled plane exists by focusing on the plane of the point source (this was achieved by placing a mirror in front of the illuminated surface and focusing the camera on the reflected image of the laser source). The method was used either as a single emulsion double exposure before and after loading, or a time-average single exposure of a fluctuating speckle pattern and subsequent interrogation of the localized diffraction halo, where the diffraction halo associated with the blurred (vibrating) area is low. Later, Wong et al. [22] showed how the method can be combined with an optical shearing lens and CCD camera to visualize anti-nodal fringes and zero surface-strain isolines. Two speckle patterns are made to instantaneously overlap via the shearing lens and the fringe intensity is related to the tilt amplitude. Wong [23] later combined the decoupled focal plane method of Gregory with the time average imaging strategy of Spagnolo. This method has the advantages of a simplified optical setup (as it needs no shearing lens) and greater noise tolerance since it is inherently insensitive to in-plane motions due to the use of Gregory's decoupled focal plane. While this provides some insulation from ambient noises expressed as inplane disturbances, the method is still subject to ambient noise that influences surface tilt and cause localized decorrelation of the speckle patterns. Furthermore, use of this method requires a full accounting of the distance between source and camera. In most cases this should not represent a practical drawback, but one can imagine cases where this is not easily or conveniently achieved.

Herein we demonstrate an alternate method for the full-field non-contact visualization of tilt topography, i.e. the determination of anti-nodal patterns. The method relies on a local differential contrast operator to

identify regions of rapidly fluctuating tilt associated with the presence of vibrational nodes and can be considered a simplified form of the stroboscopic digital shearography technique of Hung [17], the primary simplifications being the optical image-shearing is achieved by defocusing the camera, a single time-average shearogram is used rather than two, and qualitative rather than quantitative data is determined. The absolute sensitivity of the method is primarily a direct function of the degree of defocus of the imaging system and thus can be easily modulated for a given application. Furthermore, since the method exploits the temporal difference in local contrast of a laser speckle pattern, ambient noise and vibration can be screened out a priori via a simple thresholding operation, thus revealing the superimposed vibration of interest. The method's reliance on contrast rather than the spatial distribution of individual speckles (i.e. localized correlation as in the method of Wong and Spagnolo), affords the technique virtual immunity to low-frequency motions and disturbances assuming, of course, a general equivalence exists in the speckle pattern quality everywhere in the field-of-view. Degree of contrast reduction—and therefore surface tilt—can be related to a false-color scale and superimposed on the image of the surface, making the use of the technique simple and intuitive for non-expert users. Real-time performance is achieved by exploiting the high degree of instructional parallelism that is characteristic of the laser speckle contrast analysis (LASCA) algorithm used in this study. The major drawback of the method is that the information conveyed is largely qualitative in nature. The technique is useful anywhere a simple and rapid full-field characterization of a nodal/anti-nodal distribution pattern is required. In cases where very high levels of noise and disturbance are present, we propose this method as it allows for the easy modulation of system sensitivity via a simple adjustment of camera focus (in contrast to the methods of Spagnolo and Wong which use fixed focal planes either at the object surface or the singular defocus plane proposed by Gregory). Furthermore, relatively large reference tilt fluctuations are well tolerated as the method is capable of effectively screening out most initial in-plane/out-of-plane disturbances.

2. Background

2.1. Laser speckle patterns and the LASCA algorithm

Illumination of an optically rough surface with a coherent light source (such as a laser) causes the formation of a grainy light-field known as a speckle pattern. This pattern is the direct result of the chaotic addition of countless wavelets that constitute the wavefront as they are reflected off of the microrelief of the illuminated surface. The local sum of the relative phase-shifts of these wavelets determines whether a bright speckle (constructive interference) or a dark speckle (destructive interference) results. The phase-shifts themselves arise from topography-induced optical path length differences. Coherent light speckle patterns have many interesting properties, one of which is an exquisite sensitivity to any disturbance of the illuminated object [21,24]. This property has been used in the past to quantify, with a high degree of precision and in a non-contact way, the deformation undergone by a body under load (see, for example, Ref. [1]).

Briers and Webster [25] introduced a simplified full-field method of extracting information from a laser speckle pattern. They named their method LASCA because it relates local reductions of contrast in a speckle pattern to the velocity of scattering bodies in the bloodstream of biological tissue [26,27]. In general, the contrast of a speckle pattern is given by

$$C = \frac{\sigma_I}{\bar{I}}, \tag{1}$$

where σ_I is the standard deviation of the intensity and $\bar{I}$ is the mean intensity of the speckle pattern [24]. For a fully developed speckle pattern, i.e. one whose intensity distribution follows a negative exponential, the value of the contrast is found to be 1. The technique described in this work makes use of a time-average speckle pattern captured from a vibrating surface. In practice most distributed systems under study will exhibit a range of vibration amplitudes, and this is manifest as regions of varying contrast in the imaged speckle pattern. As a result, the captured speckle pattern is only partially developed and the measured contrast is not expected to exist throughout the full range of a fully developed speckle pattern. Furthermore, should the system under study not be in an initial state of rest, the range available for speckle pattern contrast modulation by some excitation signal is even further reduced. For these reasons, we employ a methodology that computes

and stores the initial contrast values for a segmented speckle pattern in its initial state and outputs the proportional decrease in contrast at the location of each image segment.

2.2. LASCA as applied to distributed systems

We apply the LASCA technique in the form of normalized local contrast reduction measurements to locate the areas of varying surface tilt fluctuation of a vibrating distributed system. In most cases these regions correspond to the location of the vibration anti-nodes, as these are the areas that undergo the greatest oscillatory angular deflection. The method is as follows: (1) a surface of interest is illuminated by an expanded laser beam such that a speckle pattern is generated. (2) A digital video camera is used to capture and store a reference speckle pattern of the illuminated surface. (3) A calibration is performed wherein the reference speckle pattern is segmented into an XY grid of subimages of variable size (depending on the size of the speckle but typically 16×16 or 8×8 pixels) and the local contrast is computed for each subimage and stored in a look-up table. The contrast is computed in the manner outlined by He and Briers [27] and reproduced below for reader convenience, with the mean intensity defined as

$$\bar{I}(x,y)=\frac{\sum_{\mathrm{row}=0}^{(\mathrm{subheight}-1)}\sum_{\mathrm{col}=0}^{(\mathrm{subwidth}-1)}f(x+\mathrm{row},y+\mathrm{col})}{(\mathrm{subheight})(\mathrm{subwidth})}, \tag{2}$$

where subheight and subwidth are the dimensions (in pixels) of the subimage height and width, respectively, and $f(x+\mathrm{row},y+\mathrm{col})$ is the grayscale value of a given pixel at location $(x+\mathrm{row},y+\mathrm{col})$ within the subimage. The standard deviation of intensity values of a given subimage is defined [27] as

$$\sigma_I=\sqrt{\frac{\sum_{\mathrm{row}=0}^{(\mathrm{subheight}-1)}\sum_{\mathrm{col}=0}^{(\mathrm{subwidth}-1)}(f(x+\mathrm{row},y+\mathrm{col})-\bar{I})^2}{(\mathrm{subheight})(\mathrm{subwidth})}}, \tag{3}$$

at which point Eq. (1) is invoked to compute the contrast value. As the surface is presumed to have undergone minimal disturbance during this process, this establishes the maximum contrast at the location of any given subimage (in the case of a particularly noisy experimental environment the previous procedure may be repeated with the results averaged after each iteration prior to final storage in the look-up table). (4) With the initial-state look-up table complete, the camera enters a continuous acquisition loop, transferring the contents of the camera buffer to the main memory buffer of the computer for processing. (5) Each successive image undergoes the same segmentation and contrast computation process as described in the initial calibration procedure, and the normalized contrast reduction is computed using the following simple equation:

$$I_{\mathrm{table}}=\left[1-\frac{(C_{\mathrm{reference}}-C_{\mathrm{transient}})}{C_{\mathrm{reference}}}\right], \tag{4}$$

where $C_{\mathrm{reference}}$ is the computed contrast value at the initial state for a given subimage, $C_{\mathrm{transient}}$ is the computed contrast for a given subimage at some point in time during forced/passive excitation. At this point, I_{table} is used to determine an index value in a table containing a spectrum of 100 pre-computed colors used to portray the contrast reduction as a false-color image.

Using a localized normal form of the contrast operator affords this method three advantages: (1) the initial reference-state contrast is determined as a function of its spatial distribution in the optical field, thus allowing for the analysis of surfaces over which the speckle pattern quality (as determined by the absolute local contrast) varies widely, (2) a contrast "noise floor" is established that allows for thresholding and filtering-out of spurious environmental disturbances of amplitudes that would disqualify phase-dependant techniques such as holography, and (3) the computational simplicity of the method readily allows for real-time data analysis.

The inherent parallelism of the algorithm can be exploited to achieve very efficient processing. Two layers of parallelism can be applied to this algorithm: thread level and instruction level. Since the results computed for a given subimage are independent of any previous or global result, the subimages can be processed independently of each other. To accomplish this, the computer is queried upon application start-up as to the number of available processors (cores). This number determines the number of separate threads of execution that are instantiated and launched by the software. Once the threads are running, they iterate through each

image and process the subimages in a synchronized fashion that prevents any subimage from being processed twice. This results in an approximate $2\times$ increase in performance. Additional performance gains can be realized by exploiting the single instruction multiple data (SIMD) extensions available in modern CPUs [28]. These instructions act on vectors of numbers, the largest currently being 128 bits in length. Single precision floating-point computations were found to offer sufficient accuracy for this application. For 32-bit operating system, these values require 32 bits of memory, i.e. four 32-bit floating point values can be packed into a single 128-bit vector. Since the mathematical instructions operate on the entire contents of the vector, four floating-point values can be processed simultaneously. The subimage dimensions are chosen to be integer multiples of 4 (i.e. 8×8, 12×12, 16×16 pixels, etc.), to enable easy implementation of the streaming SIMD extensions (SSE). Therefore, each thread operates on a given subimage, with instructions within that subimage operating on groups of four pixels simultaneously for a theoretical improvement of $8\times$ for dual-core computers. This improvement cannot usually be achieved due to memory latency issues [28], but large performance gains are realizable nonetheless. An algorithm flowchart is shown in Fig. 1.

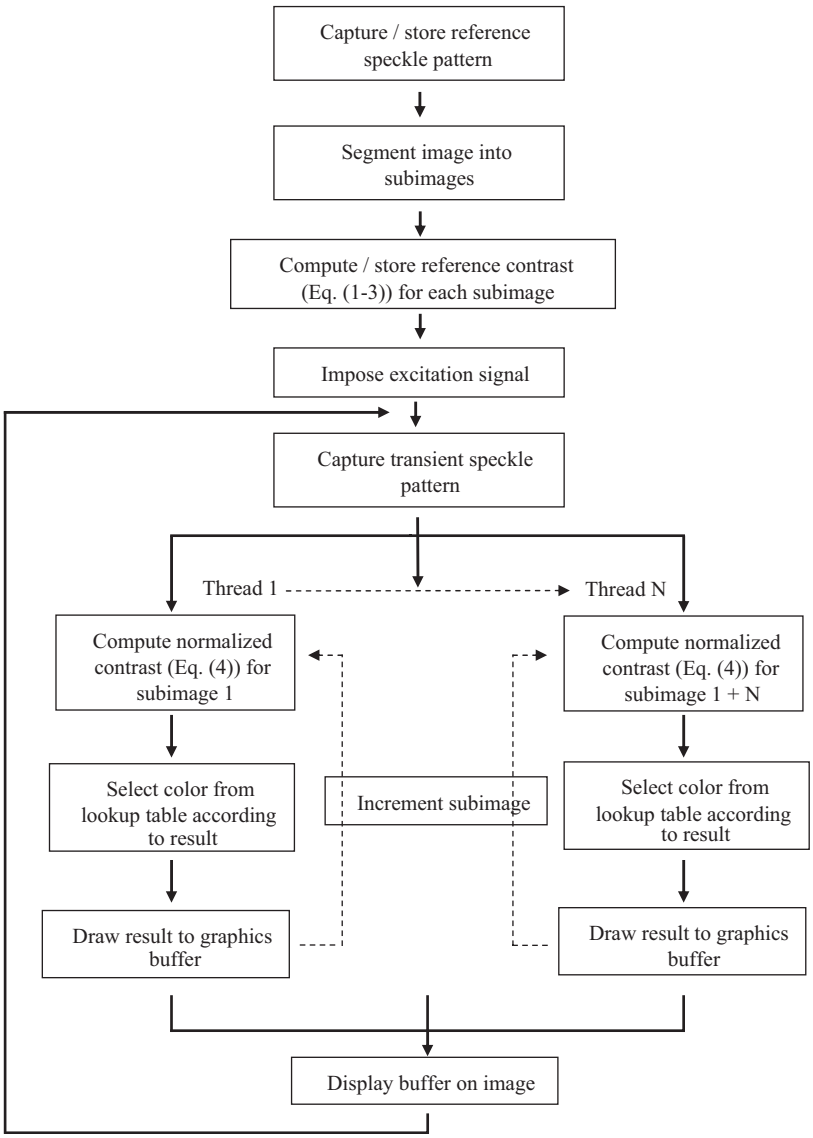

Fig. 1. Algorithm flow chart.

Since the contrast reduction is directly proportional to the magnitude of the (oscillating) tilt of a vibrating surface, this method does not generate data in the form of a fringe map corresponding to out-of-plane displacements. Rather, if we consider a continuous distributed system whose periodic out-of-plane deflection can be described (at a given moment) by some function $f(x,y)$ which is differentiable everywhere, then the fringes generated by this technique are spatially related to the gradient vector of this amplitude function, namely

$$\nabla f = \frac{\partial f}{\partial x}\vec{i} + \frac{\partial f}{\partial y}\vec{j}, \tag{5}$$

where i and j are unit vectors in the x and y directions, respectively. The center of the fringe will correspond to the greatest degree of oscillating tilt irrespective of its spatial direction—i.e. the magnitude of the gradient vector computed by

$$\|\nabla f\| = \sqrt{\left(\frac{\partial f}{\partial x}\vec{i}\right)^2 + \left(\frac{\partial f}{\partial y}\vec{j}\right)^2}. \tag{6}$$

The spatial distribution of the magnitude maximums therefore corresponds to the spatial distribution of the anti-nodes of the system.

3. Simulation and experimental verification

For experimental verification, an acoustically excited membrane, fixed on all sides, was used. The membrane consisted of a white cotton canvas mounted onto a wooden stretcher frame. Two membranes were used: a square membrane of dimensions $24 \times 24\,\text{in}^2$ and a smaller rectangular membrane of dimensions $8 \times 10\,\text{in}^2$. Two self-amplified speakers were positioned 18 in in front and on either side of the canvas for acoustic excitation via line-level output from a laptop computer. One speaker was used to generate the signal sine wave in order to induce the harmonic modes of the vibrating membrane. The second speaker was used to emit acoustic white noise to test the effectiveness of the technique in the presence of ambient noise. A Prosilica EC1380 IEEE1394 digital video camera (resolution 1360×1024 pixels, 8-bit grayscale) was used to capture images at frame rates ranging from 15–20 frames/s, depending on exposure times. The camera was positioned approximately 72 in in front of the canvas and the lens adjusted to the minimum focal distance (approximately 6 in from the front of the lens). The stretched canvas was illuminated with a 250 mW laser (532 nm, expanded using a $40\times$ microscope objective). The experimental setup is shown in Fig. 2.

In order to precompute the nodal shape maps of these vibrating membranes, we focus on the characteristic shape function of the predictive equation and exclude other physical parameters (density, tension, etc.), other than the fixed boundary condition. The shape function for a perfect membrane is given [29] as

$$f(x,y) = \sin\left(\frac{m\pi x}{a}\right)\sin\left(\frac{n\pi y}{b}\right), \quad m,n = 1,2,\ldots, \tag{7}$$

where a, b are the dimensions of the membrane and x and y are unit distances along the membrane's orthogonal axes. Differentiating Eq. (7) with respect to the two independent variables yields

$$\frac{\partial f}{\partial x} = \sin\left(\frac{m\pi y}{b}\right)\cos\left(\frac{m\pi x}{a}\right)\frac{m\pi}{a}, \tag{8a}$$

$$\frac{\partial f}{\partial y} = \sin\left(\frac{m\pi x}{a}\right)\cos\left(\frac{n\pi y}{b}\right)\frac{n\pi}{b}. \tag{8b}$$

The magnitude of the gradient vector is then

$$\|\nabla f\| = \sqrt{\left(\sin\left(\frac{m\pi y}{b}\right)\cos\left(\frac{m\pi x}{a}\right)\frac{m\pi}{a}\right)^2 + \left(\sin\left(\frac{m\pi x}{a}\right)\cos\left(\frac{n\pi y}{b}\right)\frac{n\pi}{b}\right)^2}. \tag{9}$$

Solving Eq. (9) for independent variables x and y gives the magnitude of the gradient vector everywhere on the membrane for a given combination of nodal lines m and n. For the purposes of experimental verification,

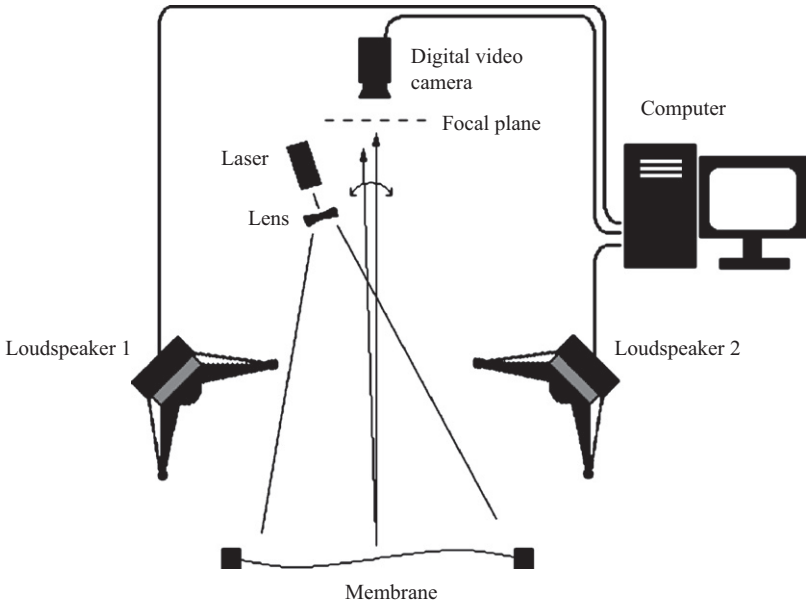

Fig. 2. Experimental setup.

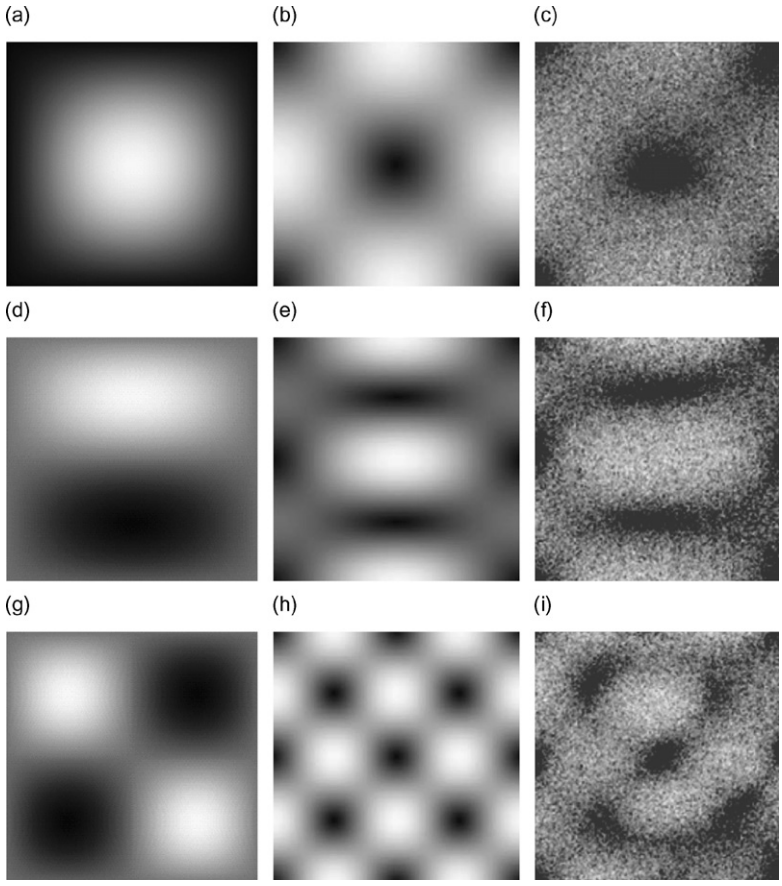

Fig. 3. (a) Mode 1,1 (deflection), (b) mode 1,1 (gradient). (c) mode 1,1 (imaged), (d) mode 2,1 (deflection), (e) mode 2,1 (gradient), (f) mode 2,1 (imaged), (g) mode 2,2 (deflection), (h) mode 2,2 (gradient) and (i) mode 2,2 (imaged).

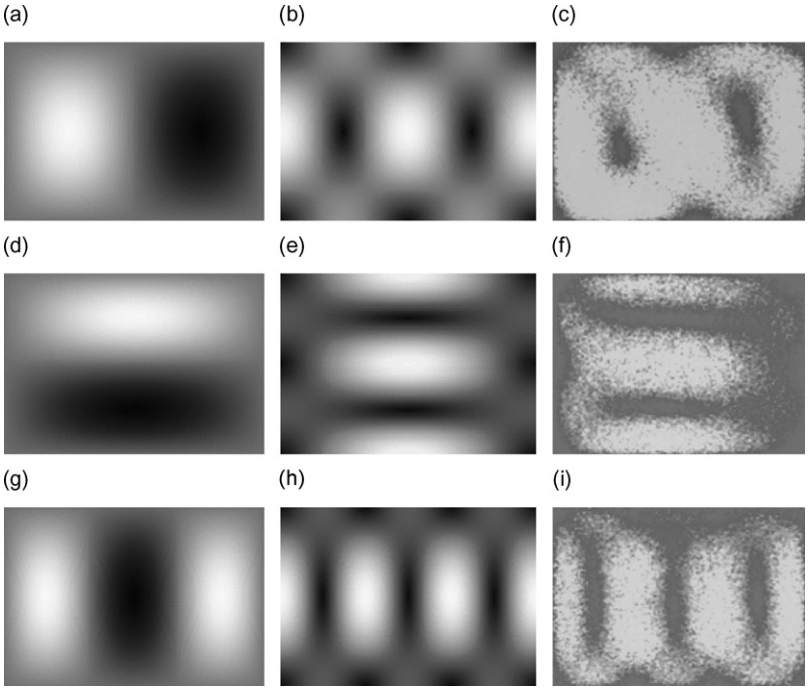

Fig. 4. (a) Mode 1,2 (deflection), (b) mode 1,2 (gradient), (c) mode 1,2 (imaged), (d) mode 2,1 (deflection), (e) mode 2,1 (gradient), (f) mode 2,1 (imaged), (g) mode 1,3 (deflection), (h) mode 1,3 (gradient) and (i) mode 1,3 (imaged).

the distribution of the gradient vector magnitudes for a selection of characteristic modal shape functions of a vibrating membrane is solved theoretically via computer and displayed as grayscale maps. The viability of the contrast speckle technique is evaluated by scanning through a band of acoustic frequencies to identify the appearance of a given gradient map as predicted by solution to Eq. (9). Fig. 3 shows three results for the square membrane, while Fig. 4 shows three results for the smaller rectangular membrane. In all cases the theoretical predictions are shown for comparison. For the square membrane used in this study, the fundamental mode (mode 1,1) occurred at a frequency below the usable frequency response of the loudspeaker. This mode was induced via an impulse excitation at the center of the membrane while imaging the ring-down pattern. Good agreement with theoretical predictions for the three selected modes can be seen for both membranes.

To evaluate the effectiveness of the technique in the presence of ambient noise, a mode was identified via acoustic sine-wave sweep (mode 3,1) at 90 dB SPL (Fig. 5a) on the square membrane so as to provide a readily identifiable pattern for visual evaluation. A slightly rotated fringe pattern of the predicted shape can be seen (the rotation most likely caused by a state of anisotropic tension in the canvas). The signal was then muted and acoustic white noise was emitted from loudspeaker 2 at an SPL of 105 dB (Fig. 5b). While maintaining the noise emission, the acoustic sine wave emission from loudspeaker 1 was restored. The result, as seen in Fig. 5c, is to superimpose a degree of noise onto the mode 3,1 fringe pattern, thus obscuring the fringes. By adjusting the contrast ratio threshold level while monitoring the computer screen output as described in Section 2 (adjusting the "$C_{\text{reference}}$" value of Eq. (4) to correspond to the noise floor), the noise is masked and the fringe visibility is restored (Fig. 5d).

4. Conclusion

A simple technique for imaging the anti-nodes of vibrating systems has been shown. The method requires little in the way of equipment other than a computer, laser and inexpensive digital video camera. Virtually no

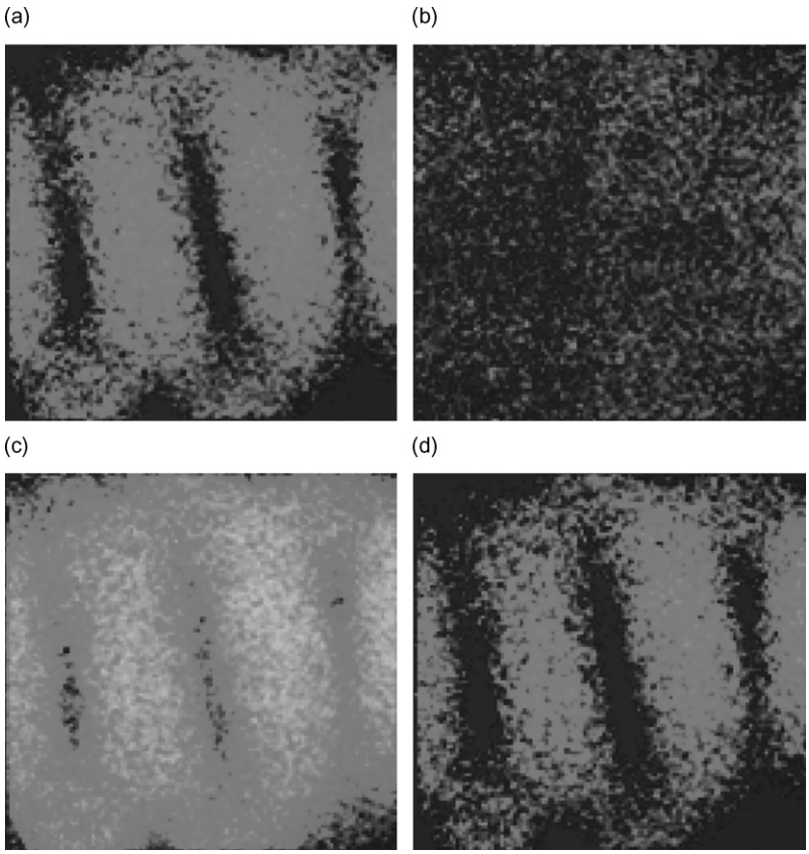

Fig. 5. (a) Membrane disturbance (mode 1,3) with acoustic sine wave excitation at 90 dB, (b) membrane disturbance with acoustic white noise excitation at 105 dB, (c) membrane disturbance with simultaneous 90 dB sine wave signal and 105 dB white noise and (d) same as (c) but with noise masked by thresholding operation.

user expertise is required to implement this method, and lasers of low beam quality (i.e. inexpensive) are sufficient for this application. The algorithm used to process the speckle patterns is computationally efficient and inherently parallel, allowing for real-time processing of high-resolution images. The method enjoys a high tolerance for environmental noise through its contrast thresholding facility, while the system sensitivity is easily adjusted by modulating the degree of camera defocus as required. As the sensitivity is directly related to defocus, the system sensitivity is not theoretically wavelength limited. The practical limitations to sensitivity of this technique are, ultimately, noise tolerance and space requirements. General drawbacks of the method are primarily twofold: (1) it does not directly image nodal patterns, but rather the anti-nodes (the location of the nodes can usually be inferred from the anti-node map), and (2) the information provided by the method is qualitative rather than quantitative. In noting that the degree of contrast reduction is directly related to the amplitude of the oscillation, it may be possible to construct a relationship between the contrast reduction and the initial contrast/exposure time/oscillation speed/focal distance/etc., to extract the analytic tilt topography of the surface. The method outlined here should prove useful in cases where the spatial distribution of nodes/anti-nodes of large systems needs to be determined quickly (for the placement of dampeners or sensors, as an example) under noisy uncontrolled conditions.

References

[1] V.P. Shchepinov, V.S. Pisarev (Eds.), *Strain and Stress Analysis by Holographic and Speckle Interferometry*, Wiley, West Sussex, 1996.
[2] C.-H. Huang, C.-C. Ma, Experimental measurement of mode shapes and frequencies for vibration of plates by optical interferometry method, *Journal of Vibration and Acoustics* 123 (2001) 276–284.

[3] G.S. Spagnolo, Electronic speckle pattern interferometry: an aid in cultural heritage protection, *Trends in Optics* 3 (1996) 299–326.
[4] D.C. Ghiglia, M.D. Pritt, *Two-dimensional Phase Unwrapping: Theory, Algorithms, and Software*, Wiley, New York, 1998.
[5] L.-S. Wang, S. Krishnaswamy, Additive-subtractive speckle interferometry: extraction of phase data in noisy environments, *Optical Engineering* 35 (1996) 794–801.
[6] H.A. Bruck, S.R. McNeill, M.A. Sutton, W.H. Peters III, Digital image correlation using Newton–Raphson method of partial differential correction, *Experimental Mechanics* 29 (1989) 261–267.
[7] T.C. Chu, W.F. Ranson, M.A. Sutton, W.H. Peters, Applications of digital-image-correlation techniques to experimental mechanics, *Experimental Mechanics* 25 (1985) 232–244.
[8] F. Jin, F.P. Chiang, A new technique using digital speckle correlation for nondestructive inspection of corrosion, *Material Evaluation* 55 (1997) 813–816.
[9] F. Jin, F.-P. Chiang, ESPI and digital speckle correlation applied to inspection of crevice corrosion on aging aircraft, *Research in Nondestructive evaluation* 10 (1998) 63–73.
[10] G. Vendroux, W.G. Knauss, Submicron deformation field measurements: part 2. Improved digital image correlation, *Experimental Mechanics* 38 (1998) 86–92.
[11] F.-P. Chiang, K.-C. Chin, W.-B. Chang, Time average laser specklegram of plate vibration using multi-aperture recording, *Applied Optics* 20 (1981) 1123–1124.
[12] F.-P. Chiang, R.-M. Juang, Laser speckle interferometry for plate bending problems, *Applied Optics* 15 (1976) 2204–2219.
[13] F.-P. Chiang, R.-M. Juang, Vibration analysis of plate and shell by laser speckle interferometry, *Optica Acta* 23 (1976) 997–1009.
[14] F.-P. Chiang, C.J. Lin, A Lidenberg method for plate bending studies using laser speckles, *Mechanics Research Communications* 7 (1980) 241–246.
[15] G.S. Spagnolo, D. Paoletti, Laser speckle correlation for monitoring building stone efflorescences, *Journal of Optics (Paris)* 27 (1996) 133–137.
[16] G.S. Spagnolo, D. Paoletty, P. Zanetta, Local speckle correlation for vibration analysis, *Optics Communications* 123 (1996) 41–48.
[17] Y.Y. Hung, A speckle-shearing interferometer, *Optics Communications* 11 (1974) 132–135.
[18] Y.Y. Hung, Shearography: a new optical method for strain measurement and nondestructive testing, *Optical Engineering* 21 (1982) 391–395.
[19] Y.Y. Hung, Digital shearography and applications, in: P.K. Rastogi, D. Ianudi (Eds.), *Trends in Optical Non-destructive Testing and Inspection*, Elsevier, London, 2000.
[20] D.A. Gregory, Basic physical principles of defocused speckle photography: a tilt topology inspection technique, *Optics and Laser Technology* (1976) 201–213.
[21] H.J. Tiziani, A study of the use of laser speckle to measure small tilts of optically rough surfaces accurately, *Optics Communications* 5 (1972) 271–276.
[22] W.O. Wong, K.T. Chan, T.P. Leung, Identification of antinodes and zero-surface-strain contours of flexural vibration with time-averaged speckle pattern shearing interferometry, *Applied Optics* 36 (1997) 3776–3784.
[23] W.O. Wong, Vibration analysis by laser speckle correlation, *Optics and Laser Technology* 28 (1997) 277–286.
[24] J.W. Goodman, *Speckle Phenomena in Optics: Theory and Applications*, Roberts and Company Publishers, Englewood, 2007.
[25] J.D. Briers, S. Webster, Laser speckle contrast analysis (LASCA): a nonscanning, full-field technique for monitoring capillary blood flow, *Journal of Biomedical Optics* 1 (1996) 174–179.
[26] J.D. Briers, G. Richards, X.W. He, Capillary blood flow monitoring using laser speckle contrast analysis (LASCA), *Journal of Biomedical Optics* 4 (1999) 164–175.
[27] X.W. He, J.D. Briers, Laser speckle contrast analysis (LASCA): a real-time solution for monitoring capillary blood flow and velocity, *SPIE Conference on Physiology and Function from Multidimensional Images*, San Diego, CA, 1998, pp. 98–107.
[28] *Intel 64 and IA-32 Architecture Optimization-Reference Manual*, 2007.
[29] L. Meirovitch, *Principles and Techniques of Vibrations*, Prentice-Hall, Inc., Upper Saddle River, 1997.